Chemically activated high grade nanoporous carbons from low density renewable biomass (Agave sisalana) for the removal of pharmaceuticals

Ana Mestre, Fabian Hesse, Cristina Freire, Conchi O Ania, Ana Carvalho

Mestre AS, Hesse F, Freire C, Ania CO, Carvalho AP, Chemicall activated high grade nanoporous carbons from low density renewable biomass for the removal of pharmaceuticals, J Colloids Interf. Sci, 536 (2019) 681–693.

hal-02108468v1

Chemically activated high grade nanoporous carbons from low density renewable biomass (*Agave sisalana*) for the removal of pharmaceuticals

Ana S. Mestre[1,2*], Fabian Hesse[1], Cristina Freire[2], Conchi O. Ania[3,4], Ana P. Carvalho[1*]

[1] Centro de Química e Bioquímica and Centro de Química Estrutural, Faculdade de Ciências, Universidade de Lisboa, 1749-016 Lisboa, Portugal

[2] REQUIMTE/LAQV, Departamento de Química e Bioquímica, Faculdade de Ciências, Universidade do Porto, *4169-007 Porto Portugal*

[3] Instituto Nacional del Carbón (INCAR-CSIC) 33080 Oviedo, Spain

[4] CEMHTI CNRS (UPR 3079) University of Orléans, 45071, Orléans, France

*Corresponding Author: Telephone Number +351 217500897; Fax: +351 217500088. E-mail address: asmestre@fc.ul.pt (Ana S. Mestre); ana.carvalho@fc.ul.pt (Ana P. Carvalho)

Abstract

Hypothesis

Enlarging the range of viable nanoporous carbon precursors, namely by the acid treatment of low density biomass residues, can overcome issues related with the availability and quality of raw materials that have potential impact on cost and quality grade of the final product.

Experiments

Nanoporous carbons were prepared following a two-step process: H_2SO_4 digestion/polycondensation of biomass waste (*Agave sisalana*, sisal) to obtain acid-chars that were further activated with KOH or K_2CO_3. Selected synthesized nanoporous carbons were tested for the removal of pharmaceutical compounds - ibuprofen and iopamidol - in aqueous solutions.

Findings

The structure and density of the acid-chars are highly dependent on the concentration of H_2SO_4 used in the digestion and polycondensation steps. An adequate choice of the acid-char synthesis conditions, activating agent and contact method allowed to feature nanoporous carbons with specific surface areas ranging from 600 to 2300 $m^2\ g^{-1}$ and apparent densities reaching 600 kg m^{-3}. The adsorption capacity of a sample obtained by KOH-activation for the removal of micropollutants from water was twice higher than the value attained by golden activated carbon (Cabot-Norit) commercialized for this specific purpose.

Keywords: sisal; biomass thermochemical conversion; K_2CO_3 and KOH activation; nanoporous carbons; nitrogen adsorption isotherms; kinetic assays; equilibrium adsorption data; pharmaceutical compounds removal, ibuprofen; iopamidol.

1. Introduction

The use of residues for the production of valuable products has become a common practice in several economic sectors, as it contributes to the implementation of a circular economic strategy adopted by European Union and aligned with United Nations 2030 Agenda for Sustainable Development.

In the manufacture of activated carbons at industrial scale, the choice of the precursors is an important issue due to various aspects as price fluctuations, availability and variability of sources, that can compromise the quality and price of the final product. Coconut-shell is a key precursor in the fabrication of activated carbons [1] due to its low ash content which leads to activated carbons with low metals percentage, very good attrition resistance and generally high surface areas [2, 3]. Coal and wood are also widely used precursors; however coal-derived materials usually have large ash contents, while wood-derived granular activated carbons display poor attrition resistance. Other renewable sources (*e.g.* fruit shells and stones) are also employed at industrial scale for the manufacture of activated carbons, with less expression. From an academic point of view, the list of precursors for the preparation of activated carbons is quite large, as shown in various reviews [4-8].

The search for alternative synthetic routes that allow the preparation of high grade activated carbons from biomass residues (particularly low density biomass), is an issue of academic and industrial relevance. The use of renewable feedstocks is expected to have important environmental and economic impacts, since it allows to close the loop of many biomass wastes through their use in the production of valuable tradeable goods.

Conventional activation methods usually starts either by the carbonization of the biomass - to remove volatile matter - and further thermal treatment of the char in the presence of an oxidizing agent to develop the pore network (physical activation); or by the activation of the precursor mixed with an activating agent (chemical activation) [2].

Besides porosity, the density and hardness of the activated carbons strongly depend on the properties of the precursor, with low density ones typically leading to low density and soft (low attrition resistance) carbons [9].

Alternative carbonization and activation approaches have been largely explored for the past decades aiming at reducing the energy consumption, while producing highly porous activated carbons with controlled pore architectures. Among them, the hydrothermal carbonization of polysaccharides followed by the activation of the hydrochar has emerged as an interesting method that allows the preparation of superactivated carbons [10-13] with microspherical morphology [12-14] and improved performance for various applications (e.g., energy storage/production, gas adsorption) [11, 14-16]. On the other hand, two of the main constituents of lignocellulosic biomass, *i.e.* cellulose and hemicellulose, are complex structures composed by saccharic units (pentoses and hexoses). Therefore, following a similar approach, it is possible to obtain a char after the acid digestion and polycondensation of biomass [17]. Such acid-char may be used as carbon rich precursor for the synthesis of activated carbons.

In this study, a series of high grade nanoporous carbons were prepared from the acid digestion and polycondensation of a biomass residue (*Agave sisalana*), and evaluated for the removal of emerging pollutants from aqueous solution (i.e. ibuprofen and iopamidol). The acid-chars obtained after the acid digestion and polycondensation of the biomass were chemically activated using KOH and K_2CO_3. The effect of the acid digestion conditions in the apparent density, porosity and composition of both the acid-chars and their corresponding nanoporous carbons after chemical activation was investigated. The resulting nanoporous carbons displayed moderate to high surface area with some samples outperforming a commercial benchmark carbon for the removal of pharmaceutical compounds – ibuprofen and iopamidol – from aqueous solution.

2. Experimental section

2.1 Synthesis of the acid-chars

Sisal (*Agave sisalana*) residues received from a rope industry (Cordex, Portugal) were used as raw precursor. This biomass is composed by (wt./wt.) 65.8% of cellulose, 12.0% of hemicellulose, 9.9% of lignin, 0.8% of pectin, and 0.3% of wax and water soluble compounds [18]; therefore about 78% of its structure is constituted by saccharic units. The synthesis of the sisal-derived acid-chars was inspired in the work of Wang *et al.* [19] on other biomass precursor (*i.e.* rice husk). Briefly, sisal fibers of ca. 1 cm long were digested under stirring in H_2SO_4 solutions (Sigma-Aldrich, 95-98%) for 15 min in the case of 12 and 13.5 M solutions, and for 30 min in the case of 9 M solutions. In all cases a 1:10 wt./v ratio (g of sisal to cm^3 of H_2SO_4 solution) was used and the treatment was carried out at 50 ºC, controlled by a water bath (VWR Scientific Model 1201). After the acid digestion, the solid residue (undigested sisal fibres) was removed, and the dark acidic liquor was then heated at 90 ºC under reflux during 6 h, to allow the polycondensation reactions rendering a solid product (acid-char). The polycondensation was carried out using acid concentrations equal or lower than those used in the digestion step. With exception of the acid-char prepared with H_2SO_4 13.5 M in both digestion and polycondensation steps additional 5 cm^3 of acid (same concentration as in the digestion step) or water were added per gram of biomass used. The acid-char was recovered by filtration, washed with distilled water until neutral pH, dried at 100 ºC overnight and crushed in order to get a fine powder (particles with dimensions < 0.297 mm). The sisal-derived acid-chars were labelled as SX/Y, where X and Y correspond to the H_2SO_4 concentration (M) used in the digestion and the polycondensation step, respectively (*e.g.* S9/9).

128 *2.2 Chemical activation of the acid-chars*

129 The acid-chars were activated with KOH or K_2CO_3, using various contacting methods,
130 acid-char:activating agent ratios and activation temperatures. Two methods were used to
131 allow the contact between the acid-char and the chemical activating agent: physical
132 mixing of both powders in a mortar, and solution impregnation. In the former, the
133 activation was carried out by mixing 1 g of the acid-char with K_2CO_3 (Aldrich, 99 %) or
134 KOH (Panreac, 85 %) in a weight ratio of 1:3 (acid-char:activating agent). In the case of
135 solution impregnation, the activating agent is dissolved in water, mixed with the acid-
136 char and stirred for 2 h at room temperature; the suspension was then dried at 80 ºC to
137 allow the evaporation of the excess water and crushed before the carbonization. The
138 activation was performed at 700 or 800 ºC for 1 h in a horizontal furnace (Thermolyne,
139 model 21100) under a N_2 flow of 5 $cm^3 s^{-1}$ and using a heating rate of 10 ºC min^{-1}. After
140 cooling down to room temperature under N_2 flow, the materials were washed with
141 distilled water until neutral pH, dried overnight at 100 ºC, crushed to a fine powder
142 (particles with dimensions < 0.297 mm).

143 Activated carbons were labelled after the corresponding acid-chars followed by the
144 activating agent (C for K_2CO_3, and H for KOH) and its amount per gram of acid-char
145 (in g). Unless otherwise stated, samples were prepared by physical mixture and
146 activated at 800 ºC. The activated carbons prepared by solution impregnation were
147 labelled with (s). As an example, sample S13.5/13.5/C3(s) corresponds to the carbon
148 prepared by activation of acid-char S13.5/13.5 at 800 ºC using 3 g of K_2CO_3 and
149 solution impregnation.

150 *2.3 Characterization of the materials*

Apparent -tapped- densities of the carbons were determined through a methodology adapted from the literature for powdered materials with 90 % of particles with dimensions lower than 0.177 mm (80 mesh) [20-22]. Briefly, a graduated cylinder was filled with a known amount (typically 0.5 g) of the powdered carbon (Mettler Toledo AB204-S/FACT), tapped in a rubber pad for several minutes until no further settling was observed, and the volume was recorded. The densities presented correspond to the mean value of at least three assays. The apparent densities were determined on a dry basis according to equation (1).

$$density = 1000 \times \frac{weight\ of\ sample, in\ g}{volume\ of\ sample, in\ cm^3} \times \frac{(100 - \%\ moisture)}{100} \qquad \text{Eq. 1}$$

The morphology of selected samples was evaluated by Scanning Electron Microscopy (SEM) performed at a Zeiss Supra 55 VP apparatus using 5 kV as accelerating voltage. Scanning was performed in situ on a sample powder without coating. The crystallinity of selected samples was assessed by X-ray powder diffraction (XRD) data obtained in a Pan Analytical PW3050/60X´Pert PRO apparatus equipped with a X´Celerator detector and with automatic data acquisition (X´Pert Data Collector (v2.0b) software). The diffractograms were collected at room temperature using monochromatized CuKα radiation as incident beam (40 kV-30 mA), the 2θ range of 5º to 60º was scanned with a step size of 0.017º and a time per step of 0.6 s.

The chemical composition of selected acid-chars was obtained by elemental analysis (CHNSO) using LECO CHNS-932 and LECO VTF-900 (for direct oxygen quantification) automatic analysers. Data is expressed in dry basis since the samples were previously dried at 105 ºC. Diffuse reflectance infrared Fourier transform (DRIFT) spectroscopy was recorded in a Nicolet Magna-IR560 spectrometer provided with a high sensitivity mercury cadmium telluride detector (MCT-A) that operates at cryogenic

175 temperature. Spectra were recorded on powder samples without KBr addition. Each
176 spectrum was obtained from the accumulation of 256 scans, recording with a spectral
177 resolution of 2 cm^{-1} in the mid-IR (4000-650 cm^{-1}) spectral range. The pH at the point
178 of zero charge (pH_{PZC}) of the samples was measured following the reverse mass titration
179 method [23] and using a Symphony SP70P pH meter. The thermal analysis (Setaram
180 Labsys) was carried out on ca. 10-25 mg of sample under a nitrogen flow rate of 50 cm^3
181 min^{-1}, a heating rate of 15 ºC min^{-1} and up to a final temperature of 900 ºC. The ash
182 content was determined after exposure of the samples at 600 ºC in air, until constant
183 mass.

184 The porosity of the samples was characterized by equilibrium adsorption/desorption
185 isotherms of N_2 at -196 ºC and CO_2 at 0 ºC measured in volumetric analysers from
186 Micromeritics (ASAP 2010 and Tristar 3000, respectively). The samples (60-100 mg)
187 were previously outgassed at 120 ºC for 17 h under vacuum (pressure < 10^{-2} Pa). Data
188 from the N_2 isotherms were used to estimate the apparent surface area, A_{BET}, by the
189 Brunauer-Emmett-Teller (BET) method, following the IUPAC [24, 25] and ISO 9277
190 [26] recommendations for the determination of this parameter in microporous solids.
191 The relative pressure range for the determination of the BET area was selected
192 according with two criteria: (i) positive line intersect of multipoint BET fitting ($C > 0$)
193 and (ii) maximum p/p^0 value limited to the pressure range where $n_{ads}(1-p/p^0)$
194 continuously increases with p/p^0 [25]. The total pore volume, V_{total}, was assessed using
195 the Gurvich rule [27], that is, the number of N_2 moles adsorbed at relative pressure close
196 to unity (*i.e.* $p/p^0 = 0.975$) converted in total pore volume assuming that the pores are
197 filled with the condensed N_2 in the normal liquid state. The α_s method was also applied
198 to the N_2 adsorption data, taking as reference the isotherm reported by Rodríguez-
199 Reinoso *et al.* [28], enabling to quantify the total micropore volume, $V_{\alpha\ total}$, and also the

ultra, $V_{\alpha\ ultra}$, and supermicropore, $V_{\alpha\ super}$, volumes. The total micropore volume (width < 2.0 nm) was obtained by back extrapolation of the α_s plots linear region at high relative pressure (α_s > 1) while the ultramicropore volume (width < 0.7 nm) was evaluated by the interception of the linear range defined by the experimental data between p/p^0 of 0.02 and, about, 0.4. The supermicropore volume (0.7 < width < 2.0 nm) corresponds to the difference $V_{\alpha\ total}$ - $V_{\alpha\ ultra}$. The microporosity was also quantified by applying the Dubinin-Radushkevich (DR) equation to the N_2 and CO_2 adsorption data ($W_{0\ N2}$ and $W_{0\ CO2}$, respectively). The pore size distribution (PSD) analysis in the micro-mesopore range was calculated from the N_2 adsorption data using the 2D-NLDFT-HS model that assumes surface heterogeneity and slit geometry of pores in activated carbons [29]. The micropore size distributions (MPSD) were further assessed from CO_2 adsorption data according to the method proposed by Pinto *et al.* [30] that is a variation of the DR equation which does not imposes constrains to the shape of the distribution.

2.4 Liquid phase adsorption assays

Selected acid-char derived activated carbons were tested along with a commercial benchmark carbon for the removal of two pharmaceutical compounds (PhCs) -ibuprofen and iopamidol- from aqueous solution. The commercial activated carbon - Norit SAE Super (NS) - from Cabot is a powdered material specially developed for wastewater treatment. According to the general characteristics reported in the datasheet provided by the supplier, carbon NS has an apparent (tapped) density of 425 kg m^{-3}, ca. 97 % of the particles have sizes lower than 150 µm, and displays a basic character. Ibuprofen (sodium salt, Sigma-Aldrich – Lot BCBC9914V) and iopamidol (Hovione - Lot 163926HQ01324) solutions were prepared with ultra-pure water without pH

adjustment. The solutions have a pH value around 5. About 6 mg of activated carbon and a given volume of ibuprofen or iopamidol solution were mixed in glass vials maintained at 30 ºC (water bath, Grant GD100 controller) and stirred at 700 rpm (multipoint agitation plate Poly, Variomag). Samples were collected after the desired contact time (see details in Table 1). After removing the activated carbon by filtration, the amount of ibuprofen or iopamidol remaining in solution was determined by UV-vis spectrophotometry (Genesys 10S) at the wavelength of maximum absorbance (ca. 221 and 242 nm for ibuprofen and iopamidol, respectively). The PhC uptake was calculated using the equation:

$$q_t = \frac{C_0 - C_t}{W} \times V \qquad \text{Eq. 2}$$

where q_t is the amount (mg g^{-1}) of PhC adsorbed at time t, C_0 is the initial and C_t is the PhC concentration at time t (mg dm^{-3}), V is the volume of PhC solution (dm^3) and W is the weight (g) of dried carbon.

Screening adsorption tests, as well as kinetic and equilibrium assays were performed in the experimental conditions summarized in Table 1 (mass, contact time, initial concentration, volume). Given data correspond to the average value obtained in three independent assays. Kinetic data were fitted to the linear forms of the pseudo-first and pseudo-second order kinetic models [31] while the equilibrium adsorption data were analysed considering the non-linear equations of the Langmuir [32] and Freundlich [33] isotherm models.

Table 1. Experimental conditions and activated carbons used in the screening, kinetic and equilibrium adsorption assays for the removal ibuprofen and iopamidol.

Assay	**Activated carbons**	**Conditions**			
		m_{AC} (mg)	**V_{PhC} (cm^3)**	**$[PhC]_0$ (mg dm^{-3})**	**Contact time**

Screening	S13.5/13.5/C3 S13.5/13.5/C3(s) S13.5/13.5/H3(s) S9/9/C3	6	30	180	18 h
Kinetics	S13.5/13.5/C3(s) S13.5/13.5/H3(s) NS	6	30	180	5 min to 24 h
Equilibrium Isotherms	S13.5/13.5/C3(s) S13.5/13.5/H3(s) NS	6	9 to 30	20 to 180	18 h

3. Results and discussion

3.1 Characteristics of the acid-chars

The use of different concentrations of H_2SO_4 in the digestion and polycondensation steps allowed to attain yields between 35-15 % (Figure 1(a)), being the highest value slightly higher than that reported by Wang *et al.* [17] for rice husks in similar experimental conditions. As seen, the concentration of sulphuric acid must be of at least 12 M in the digestion step, and 9 M in the polycondensation to reach yields above 30 %; otherwise the yield dropped abruptly to 15 %. The elemental analysis data (Table S1) confirmed the enrichment in carbon content and the decrease in the oxygen content of the acid-chars, compared to the precursor. Despite the differences in the yields, the composition of the acid-chars was quite similar (*i.e.*, 63 wt.% C, 4 wt.% H, 0.1 wt.% N, 0.23-0.41 wt.% S, and 32 wt.% O) and close to that of the rice husk-derived chars reported in the literature using a similar procedure [19].

The use of different H_2SO_4 concentrations seemed to have a small influence in the thermal stability of the samples, as inferred from the thermogravimetric profiles (Figure 1(b)). The TG/DTG curves of the acid-chars present two weight loss steps: the first peak appearing below 150 ºC is attributed to moisture loss, while the second one between 200 and 800 ºC corresponds to the main mass loss (ca. 50 %), linked to evolution of the

volatile matter remaining in the acid-chars. The pattern of the second peak features a shoulder at around 280 ºC corresponding to the decomposition of labile (acidic) groups; the main loss at about 400 ºC can be assigned to the decomposition of more stable oxygen containing functionalities and also some sulphur groups [34, 35]. These profiles are different from those of the pristine sisal fibres (S); the sharp peaks corresponding of the depolymerization of hemicelluloses, the cleavage of glucosidic linkages of cellulose and decomposition of cellulose oligomers into tars [18] are not observed in the acid-chars. This confirms the polycondensation of these monomers during the acid treatment at 90 ºC.

Regarding surface chemistry, the DRIFT spectra of samples S13.5/13.5, S13.5/9 and S9/9 (Figure 1(c)) revealed similar profiles. The acid-chars present a broad band at 3500-3200 cm^{-1}, assigned to O-H stretching vibrations in surface hydroxylic groups [36, 37]. The peaks ~2920 cm^{-1} and ~2850 cm^{-1} are assigned, respectively, to symmetric and asymmetric C–H stretching vibrations of aliphatic moieties of the acid-chars [36, 38]. The peaks centred at 1755-1734 cm^{-1} and 1637-1624 cm^{-1} can be assigned to stretching vibrations of C=O moieties in various configurations (e.g., lactones, anhydrides, ester or carboxylic acid, and quinones) [36, 37]. The shoulder around 1580-1560 cm^{-1} and the peak at 1510 cm^{-1} are assigned to aromatic ring C=C stretching; this peak is red-shifted likely due to the high density of oxygen in the materials (~32 %, Table S1) [37]. The presence of aromatic ring C=C bonds points out the increase in the aromatization degree after the acid treatment. The peak at 1473-1454 cm^{-1} can be attributed to carboxyl-carbonate structures [36, 37], and the band around 1250 cm^{-1} to ether structures (ether bridges between rings and C-O stretch in ether moieties) [37]. The peak at 955 cm^{-1} can also be assigned to C-O-C vibrations in cyclic anhydrides [37], while bands below 950

289 cm^{-1} (*i.e.* 905 cm^{-1} and 802 cm^{-1}) are characteristic of out-of-plane deformation

290 vibrations of C-H groups in aromatic structures [36].

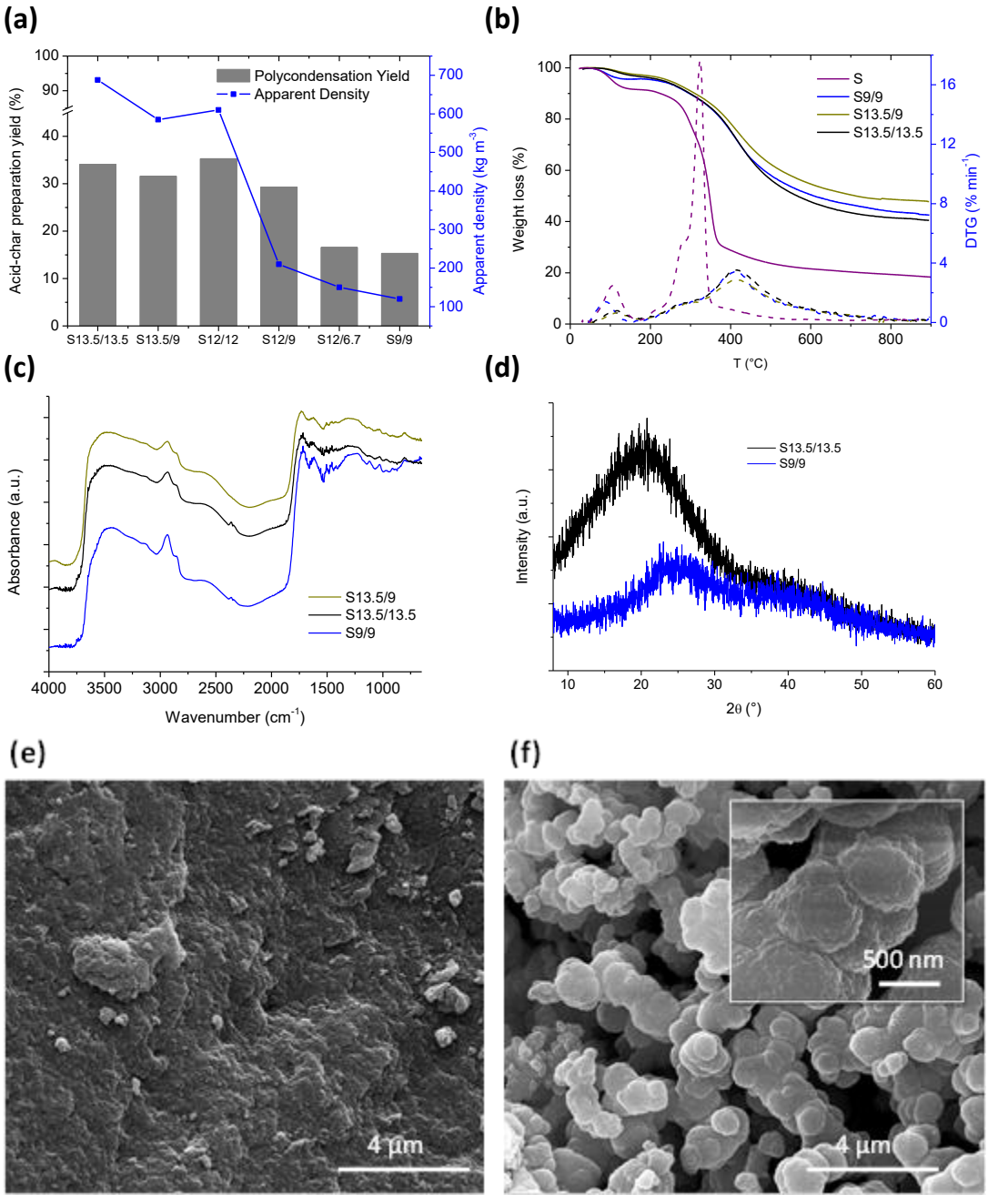

291

292

293 **Figure 1.** (a) Effect of H_2SO_4 concentration in the digestion and polycondensation steps on the

294 yields and tapped densities of the acid-chars; (b) thermogravimetric profiles (TG) and derivative

295 (DTG) curves of selected samples; (c) DRIFT spectra and (d) XRD patterns of selected acid-

296 chars. SEM images of samples (e) S13.5/13.5 and (f) S9/9 (a colour version of this figure can be

297 viewed online).

Infrared spectra also revealed the presence of sulphur moieties, in agreement with the sulphur content detected by elemental analysis. The band at 1119 cm^{-1} is assigned to stretching vibration in $–SO_3H$ and the one between 1034-1028 cm^{-1} to S=O stretching vibration. Both were more clearly observed in acid-char S9/9, and would contribute to the acidic nature of the acid-chars [38].

The acidic nature of the chars was confirmed by the low values of the pH_{PZC} (about 2 pH units), regardless the H_2SO_4 concentration used in the synthesis (Table S1). It should be highlighted that the presence of acidic oxygen groups is an important feature when envisaging further activation, as it is usually linked to a higher reactivity of the chars [6, 39]. Additionally, it will allow a good dispersion and wettability of the materials in water, favouring the contact with the activating agent in the case of solution impregnation; this will be further discussed below.

According with the XRD patterns the acid-chars have an amorphous-like carbon structure, as evidenced by the broad and low-intensity diffraction peaks (Figure 1(d)). The concentration of sulphuric acid has a low impact on the crystallinity of the samples, although, the samples prepared with the lower concentrations of acid presented lower structural order: (002) plane of graphite-like structures at ca. 20 º for S13.5/13.5 while at ca. 24º and with lower intensity for S9/9. The diffraction peak at 40 º is attributed to (101) crystalline planes of graphite in the microcrystalline regions of the carbon matrix. The shift of both peaks compared to the values of graphite (ca. ~27 º (002) and ~45 º (101) ICDD 25-284 [40]) is indicative of increased distance between crystalline plans. This could be due to the presence of oxygen and sulphur groups, as evidenced by elemental analysis, DRIFT spectra data, and acidic pH_{PZC} values of these samples (Table S1).

On the other hand, the concentration of sulfuric acid had a dramatic influence on synthesis yields, the morphology and apparent densities. In fact, digestion in H_2SO_4 13.5 M rendered high density acid-chars, regardless the concentration of acid used in the polycondensation step. In contrast, the density of the samples digested in H_2SO_4 12 M was found to follow a different trend with the concentration of acid used in the polycondensation step. High density materials were obtained when the polycondensation was carried out in H_2SO_4 12 M, with the density decreasing sharply for lower concentration of sulfuric acid (from 600 to 150 kg m^{-3}, Figure 1(a)). This behavior is certainly related with the morphological changes observed by SEM analysis (Figure 1(e) and (f)). While sample S13.5/13.5 has a compact morphology formed of small primary particles fused onto a dense and rough material, sample S9/9 is composed of interconnected spheres with diameters of around 500 nm, that originate an aerogel-like structure with an extended pore transport systems.

Summarizing, the selection of the concentration of H_2SO_4 in both digestion and polycondensation steps controls the density of the acid-char, especially for values lower than 12 M. The higher yields obtained for the synthesis carried out in 12 M (or higher) H_2SO_4 in both steps are related with a more effective extraction of the precursor's saccharic units, and a more extensive polycondensation reaction.

The N_2 adsorption data shows that the concentration of the acid does not influence the porosity of the acid-chars. All of them displayed type II isotherms (not shown) characteristic of materials with an incipient porosity [24]; accordingly, low surface area values (< 10 m^2 g^{-1}) were obtained for all the acid-chars. However, important differences were observed in the porosity of the nanoporous carbons obtained after activation of the acid-chars (see discussion below).

3.2 Characteristics of the nanoporous carbons

The textural properties and apparent densities of the nanoporous carbons prepared by activation of the acid-chars are clearly dependent on the H_2SO_4 concentrations used in the synthesis of the latter. Figure 2(a) shows the trends corresponding to samples prepared by activation using K_2CO_3 at 800 ºC of various acid-chars.

As seen in Figure 2(b) all the carbons displayed type I isotherms according to the IUPAC classification [24], indicating that they are essentially microporous materials. Despite the similarities in chemical composition and stability of the acid-chars (Table S1 and Figure 1(b)), large differences are observed in the porosity of the resulting activated carbons. Carbons prepared by activation of low density acid-chars S9/9 and S12/9 (< 200 kg m^{-3}) present at least twice the total pore volume of those prepared from high density acid-chars (> 500 kg m^{-3}). Their pore network is composed by micropores and about 13 % of mesopores. On the contrary, activated carbons S12/12/C3, S13.5/9/C3 and S13.5/13.5/C3 are predominantly microporous samples.

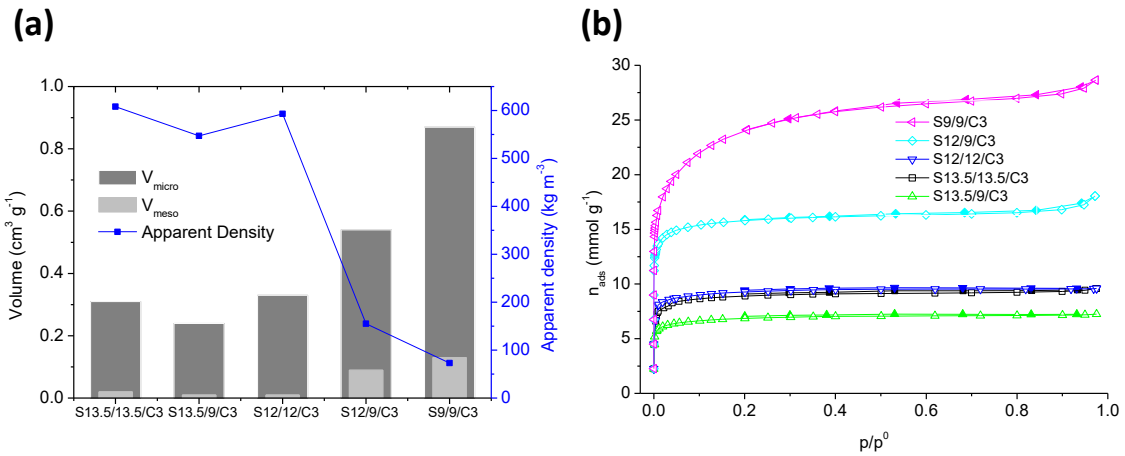

Figure 2. Properties of the activated carbons prepared by physical mixing with K_2CO_3 (3 g K_2CO_3 per gram of acid-char) followed by activation at 800 ºC during 1 h (a) micro and mesopore volumes and the influence of acid-char precursor in apparent density of the activated carbons is also displayed, (b) N_2 adsorption isotherms (a colour version of this figure can be viewed online).

To evaluate the effect of the contact method between the precursor and the activating agent, two samples S12/12 and S13.5/13.5 were prepared by activation using K_2CO_3 by

physical mixture and solution impregnation (series s). Whereas physical mixing rendered carbons with a moderate porosity development, impregnation from solution allowed the preparation of micro-/mesoporous solids, with mesopore volumes accounting for ca. 50 % of the total pore volume (Fig. 3(b) and Fig. S1). The isotherms of the carbons obtained from solution impregnation present H2(a) type hysteresis loops [24, 41], indicating complex pore structures; the desorption branch of the hysteresis loop of carbon S13.5/13.5/C3(s) is steeper than the adsorption branch, pointing out to ink-bottle shape pores and pore-blocking effects. The relative pressure of the closing end of the hysteresis loop suggests cavitation-induced evaporation effects, characteristic of samples with narrow pore necks connecting the main mesopore cavities [24, 41].

It should be pointed out that this methodology (activation of acid-chars) allowed to prepare carbons with different textural features than those obtained by chemical activation of sisal wastes-themselves [42]. These are mainly microporous carbons [42, 43] while herein described materials displayed a higher porosity development in the full micro-mesopore range, despite presenting similar global preparation yields (ca. 16-18 % for two-step and 17 % for optimized direct activation [44]).

Regarding the effect of the activating agent, the material obtained by KOH solution impregnation displayed the highest total pore volume, and a mainly micropore network as inferred from the shape of the nitrogen adsorption isotherm (type I and absence of hysteresis loop). The analysis of the pore size distribution obtained by applying the 2D-NLDFT-HS method to the N_2 adsorption data (Fig. 3(c)) confirms the dependence of the pore network characteristics with the contacting method and the activating agent. Physical mixing with K_2CO_3 and solution impregnation with KOH rendered mainly microporous carbons, whereas the carbons prepared upon solution impregnation with K_2CO_3 present a well-developed mesopore structure centered at about 7 nm.

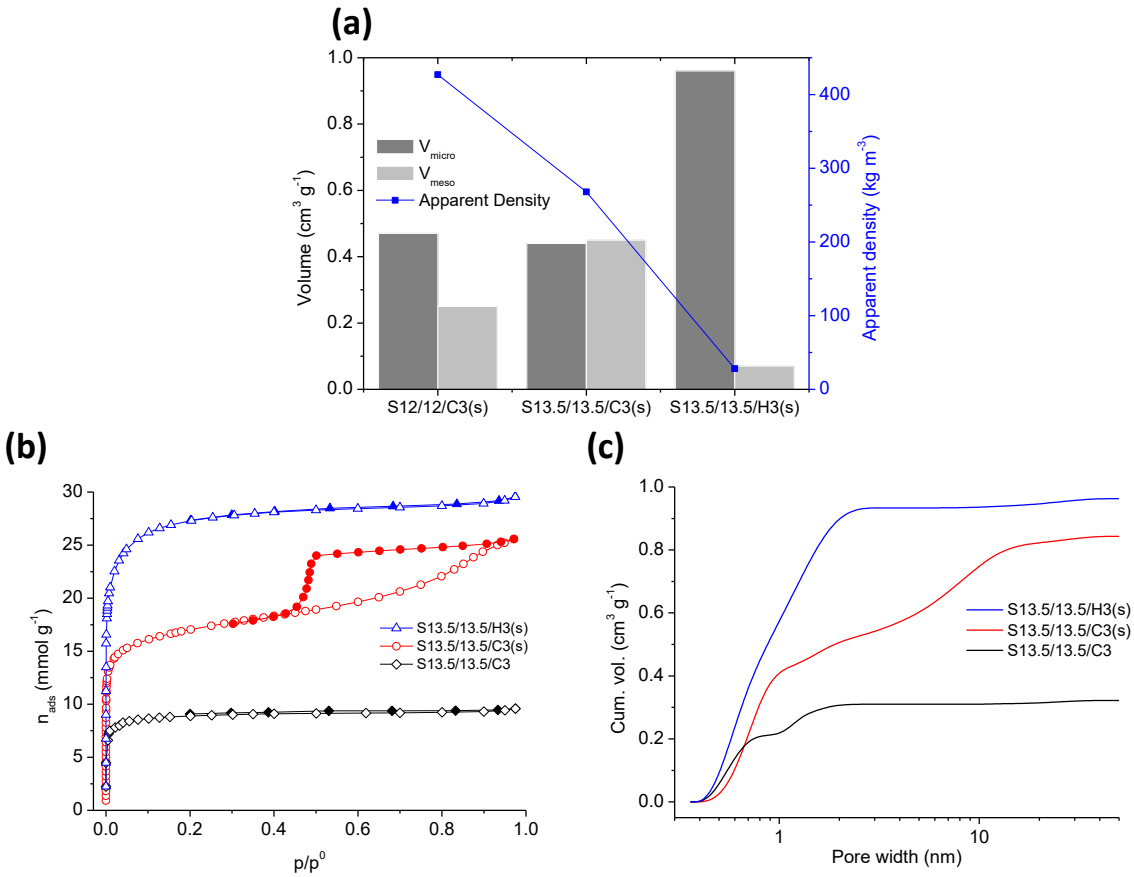

Figure 3. (a) Micro and mesopore volumes of the activated carbons prepared by solution impregnation of acid-chars S12/12 and S13.5/13.5 with K_2CO_3 or KOH (3 g activating agent per gram of acid-char) followed by activation at 800 ºC during 1 h. The influence of acid-char precursor in apparent density of the activated carbon is also displayed; (b) N_2 adsorption isotherms of activated carbons prepared from acid-char S13.5/13.5; (c) Cumulative pore size distributions obtained from the 2D-NLDFT-HS method applied to the N_2 adsorption isotherms (A colour version of this figure can be viewed online).

Regarding morphology, images in Fig. S2 reveal that the roughness of the acid-char S13.5/13.5 particles changed after activation, leading to particles with smooth and exfoliated sections certainly due to the matrix consumption during activation (activation yields around 50 %, Table 2). The XRD patterns of the activated materials (Fig. S3) reveal the expected patterns of amorphous carbons with a low structural order. Compared to the acid-chars the XRD patterns of the nanoporous carbons present slightly more intense peaks at 2θ values of ca. 25 and 44º, corresponding to the reflections of carbonaceous materials. This is associated to an increase in the

aromatization during the activation, and a low surface functionalization. In fact, both thermogravimetric analysis and infrared spectroscopy (Fig. S4) indicate that activation leads to a decrease in the surface functionalization (mass loss of *ca.* 15 wt.% for the activated carbon, compared to 56 wt.% for acid-char). Also pH_{PZC} values of samples S13.5/13.5/C3(s) and S13.5/13.5/H3(s) are less acidic than that of pristine acid-char (respectively, 3.8 and 4.9 versus 1.7).

Figure 4 shows smooth surfaces for the carbons obtained by K_2CO_3 activation using physical mixing of high density acid-chars (samples S13.5/13.5, S13.5/9 and S12/12). For the low density acid-char (sample S9/9), the activation has less effect on the morphology (Figure 4). SEM images show that the impregnation in solution with K_2CO_3 seems to originate less compact particles; this is in line with the 50 % decrease in the density in sample S13.5/13.5/C3(s) compared to S13.5/13.5/C3 (Fig. 2(a) and 3(a)), despite their similar activation yields (51 *versus* 45 %, Table 2). Activation with KOH leads to a pronounced morphological change, originating sponge-like particles that justify the very low apparent density of the final material (< 50 kg m^{-3}). Major morphology changes upon KOH activation of chars have also been reported in the literature [13, 14, 45], and can be justified by the distinct activation mechanisms between K_2CO_3 and KOH. The KOH activation reactions start at 400 ºC and lead to the formation of gases and K-compounds, which together activate the precursor; at converse, the decomposition of K_2CO_3 starts at 700-800 ºC, allowing a less extensive consumption of the matrix [46]. This fact also justifies the lower activation and global yields obtained upon KOH activation (Table 2).

The main textural parameters obtained from the analysis of N_2 isotherms at -196 ºC of the nanoporous carbons are compiled in Table 2. With exception of sample S9/9/C3, all the synthesized carbons present a wide distribution of micropores. By means of KOH

activation of high density acid-chars, or K_2CO_3 activation of low density acid-chars, it is possible to attain surface areas higher than 1900 m^2 g^{-1} and total pore volumes of 1.0 cm^3 g^{-1}. Such carbons are mainly composed of supermicropores; this is likely associated to the low activation and global yields (ca. 20 % and 3 %, respectively) and the low densities (< 100 kg m^{-3}).

The activation with KOH at 700 ºC allows higher yields but lower supermicropore volumes and still low density carbons. Compared to the carbons prepared by physical mixing, higher pore volumes and a well-developed network of mesopores are obtained upon solution impregnation with K_2CO_3. Furthermore, the activation and global yields are similar in both methods, pointing out that solution impregnation allows a more uniform and deeper penetration of the activating agent on the particles.

The microporosity was further analysed through CO_2 adsorption isotherms. The micropore size distributions presented in Figure 5 reveal that the carbons prepared by physical mixing of high density acid-chars with K_2CO_3 have narrow micropore distributions in the ultramicropore range, thus showing molecular sieve properties. The carbons prepared by solution impregnation with K_2CO_3 or KOH present monomodal and continuous distributions in the range from 0.4 to 2.0 nm. Additionally, sample S9/9/C3 have bimodal distribution of micropores. It is important to note that the commercial carbon used as benchmark for the liquid adsorption assays also presented a bimodal distribution of micropores.

Interestingly, the surface area values follow an inverse correlation with the apparent densities of the nanoporous carbons; this allows to identity three major groups of samples linked with the properties of the acid-char, the contacting methodology and the activating agent. As seen in Figure 6, a fine control of the synthesis parameters allows

457 to prepare low density superactivated carbons (> 1800 m^2 g^{-1}) and high density
458 materials with surface areas close to 800 m^2 g^{-1}.

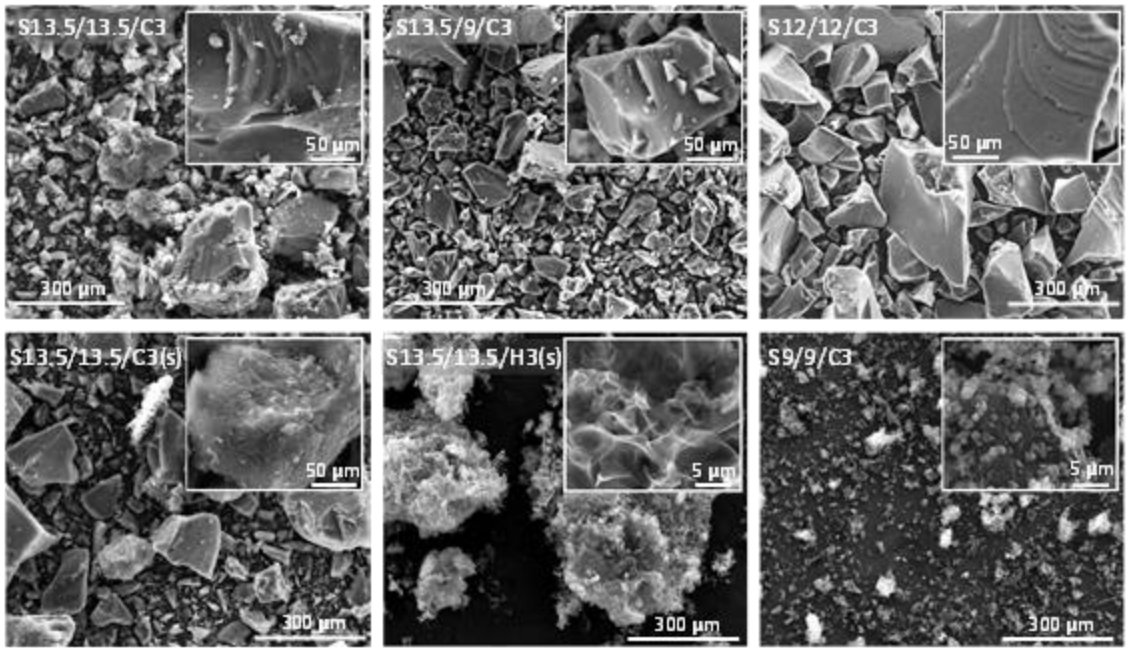

459

460 **Figure 4.** SEM images of the nanoporous carbons. The insets correspond to higher
461 amplifications to better illustrate the surface of the materials.

462

463 **Table 2**. Textural properties of the nanoporous carbons, activation and global yields.

Sample	Yield		α_s Method						DR Method	
	Activation (%)	Global (%)	A_{BET} (m^2 g^{-1})	V_{total} [c] (cm^3 g^{-1})	V_{meso} [d] (cm^3 g^{-1})	$V_{\alpha\ total}$ (cm^3 g^{-1})	$V_{\alpha\ ultra}$ (cm^3 g^{-1})	$V_{\alpha\ super}$ (cm^3 g^{-1})	$W_{DR\ N2}$ (cm^3 g^{-1})	$W_{DR\ CO2}$ (cm^3 g^{-1})
S13.5/13.5/C3	45	15	781	0.33	0.02	0.31	0.10	0.21	0.32	0.34
S13.3/13.5/C3(s)	51	18	1419	0.89	0.45	0.44	0.22	0.22	0.56	0.45
S13.5/13.5/H3(s)	20	7	2309	1.03	0.07	0.96	0.17	0.79	0.87	0.50
S13.5/13.5/H3(s/700)	33	11	1906	0.82	0.07	0.75	0.29	0.46	0.75	-
S13.5/9/C3	45	14	602	0.25	0.01	0.24	0.13	0.11	0.24	0.33
S12/12/C3	50	18	818	0.34	0.01	0.33	0.19	0.14	0.33	0.21
S12/12/C3(s)	46	16	1372	0.72	0.25	0.47	0.26	0.21	0.52	-
S12/9/C3	43	13	1391	0.63	0.09	0.54	0.33	0.21	0.53	-
S9/9/C3	20	3	1938	1.00	0.13	0.87	0.00	0.87	0.70	0.51
NS	-	-	1297	0.70	0.30	0.40	0.02	0.38	0.39	0.27

464 [a] Activation Yield = ($m_{nanoporous\ carbon}$ / $m_{acid\text{-}char}$)×100
465 [b] Global Yield = ($m_{nanoporous\ carbon}$ / m_{sisal})×100
466 [c] Evaluated at p/p^0 = 0.975 in the N_2 adsorption isotherms at -196 °C
467 [d] Difference between V_{total} and $V_{\alpha\ total}$
468
469

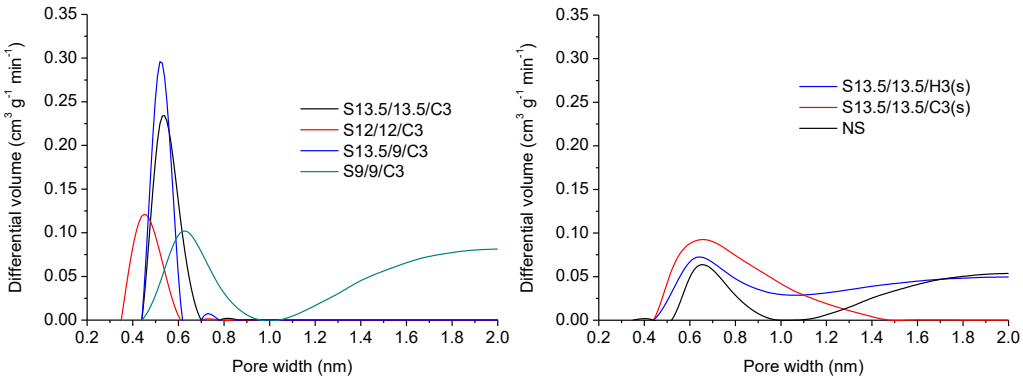

Figure 5. Micropore size distributions of the physically (left) and solution impregnated as well as commercial sample (right) obtained by fitting the CO_2 adsorption isotherms at 0 ºC to the method described by Pinto *et al.* [30]. (A colour version of this figure can be viewed online).

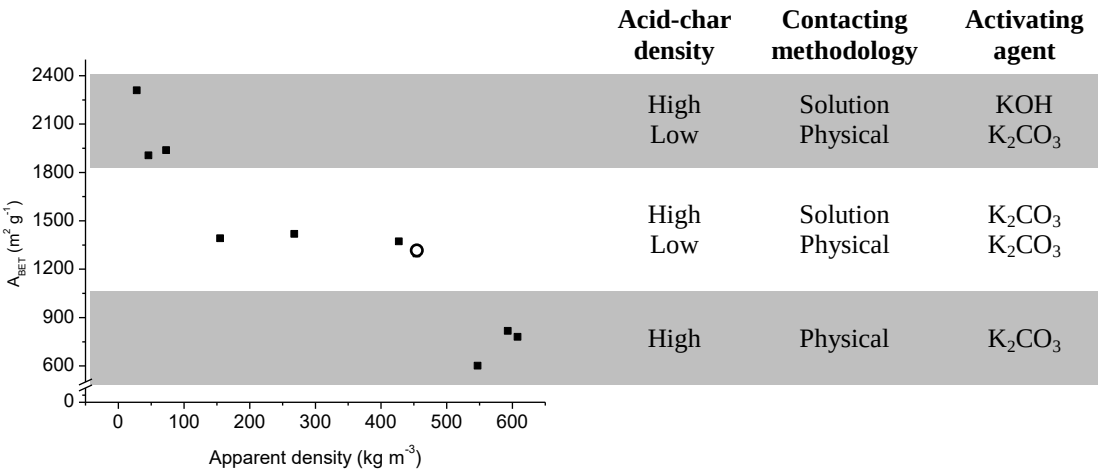

Figure 6. Correlation between A_{BET} and apparent density of the synthesized nanoporous carbons (squares) and the commercial sample (circle).

The activation of high density acid-chars with K_2CO_3 by solution impregnation also rendered materials with high surface areas (≈ 1400 m^2 g^{-1}), a well-developed micro-mesopore network, high activation and global yields (*ca.* 46-51 wt.% and 16-18 wt.%, respectively) and apparent densities close to those of commercial samples. It must be highlighted that such combination of porous features is not common by K_2CO_3 activation of low-ash content precursors.

3.3 Ibuprofen and iopamidol adsorption onto selected nanoporous carbons

Based on screening assays, four nanoporous carbons were selected for the removal of ibuprofen and iopamidol (Figure 7), two active pharmaceutical ingredients commonly detected in wastewater effluents and drinking water. The removal efficiencies after 18 h of contact time are presented in Fig. S5. Samples S13.5/13.5/C3(s), S13.5/13.5/H3(s) and S9/9/C3 attained similar ibuprofen removal efficiencies in the range 40-45 %, as opposed to the low uptake of carbon S13.5/13.5/C3 (*ca.* 25 %). For iopamidol, the removal efficiencies of the selected carbons ranged between 10-74 %, following the sequence: S13.5/13.5/H(s) > S9/9/C3 > S13.5/13.5/C3(s) > S13.5/13.5/C3. The lower uptake of carbon S13.5/13.5/C3 for both compounds can be explained by its textural features (Table 2), therefore no additional studies were performed for this sample.

Ibuprofen [47]

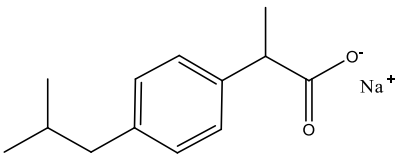

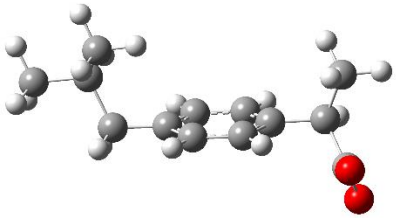

1.32 (length) × **0.72** (width) × 0.77 (thickness) in nm

Iopamidol [48]

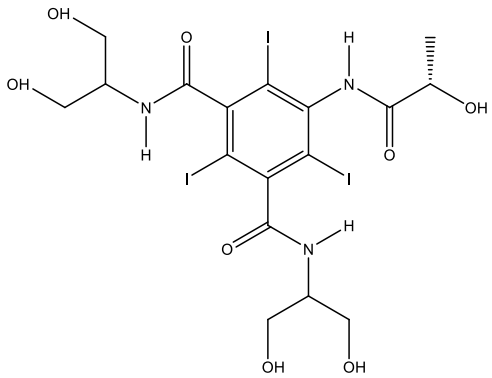

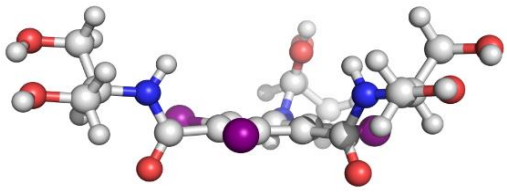

Monomer – 1.5 (length) × 1.5 (width) × **0.6** (thickness) in nm
Dimer – 1.5 (length) × 1.5 (width) × **1.2** (thickness) in nm
Trimer – **1.5** (length) × **1.5** (width) × 1.8 (thickness) in nm

Figure 7. Structure and dimensions of ibuprofen sodium salt [47] and iopamidol species [48] (critical dimensions highlighted in bold).

Based on their distinct porous features, samples S13.5/13.5/C3(s) and S13.5/13.5/H3(s) were selected for the kinetic and equilibrium assays, along with the commercial activated carbon (NS). Data presented in Figure 8 show that sample S13.5/13.5/H3(s) outperformed the commercial carbon (both in kinetic and equilibrium assays) for both compounds, whereas the comparative balance for carbon S13.5/13.5/C3(s) vs the commercial adsorbent was favourable only for ibuprofen. These results will be discussed in terms of the combined effect of porous features and surface chemistry of the materials.

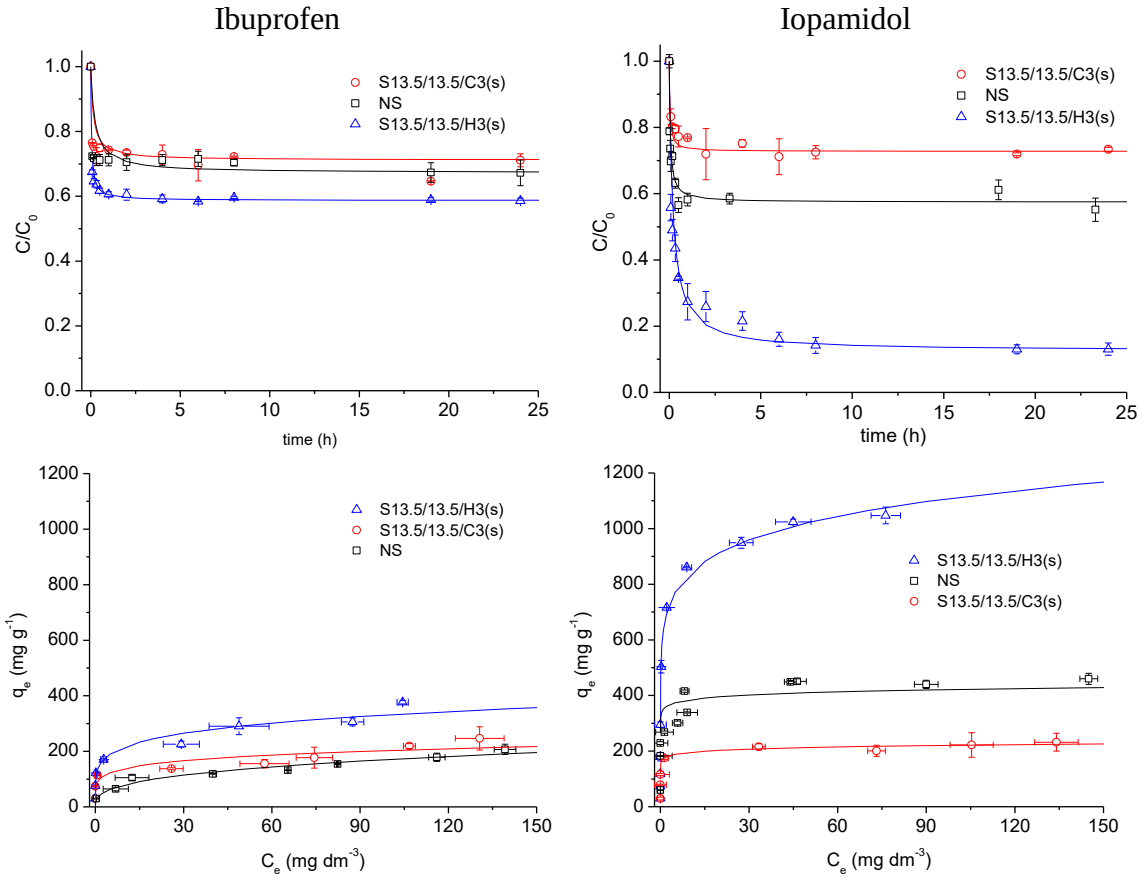

Figure 8. Kinetic results (top) and adsorption isotherms (down) of ibuprofen (left) and iopamidol (right) adsorption at 30 ºC. Symbols correspond to the experimental data while lines represent the fitting to the pseudo-second order kinetic model (top) and the fitting to the Freundlich equation (bottom). Error bars are included. Experimental conditions of the kinetic assays 6 mg carbon/30 cm^3 of pharmaceutical solution with 180 mg dm^{-3}. (A colour version of this figure can be viewed online).

512 Kinetic data was fitted to the pseudo-second order kinetic equation, with coefficients of
513 determination higher than 0.98 (Fig. 8). With the exception of the adsorption of
514 iopamidol on sample S13.5/13.5/H3(s), all the systems reached the equilibrium in about
515 3 h. According to the pseudo-second order kinetic parameters for ibuprofen adsorption
516 (Table 3) the three carbons show global adsorption rates of the same order of
517 magnitude, although slightly lower k_2 values (fast rate) were obtained for the carbons
518 containing mesopores (samples S13.5/13.5/C3(s) and NS), despite the similar uptakes.
519 The initial adsorption rate is 4.5 or 6.5 times faster in sample S13.5/13.5/H3(s) than in
520 S13.5/13.5/C3(s) and NS (respectively), pointing out the key role of the larger
521 micropores. These results are in agreement with previous data reported in the literature
522 for the adsorption of small pharmaceutical compounds (i.e. atenolol, caffeine, ibuprofen
523 acid form) on activated carbons [45, 49, 50].

524 In the case of iopamidol, the highest global adsorption rate was also attained by sample
525 S13.5/13.5/H3(s). The different iopamidol uptakes at kinetic equilibrium attained by the
526 three adsorbents limits the comparison and analysis of their initial adsorption rates since
527 this kinetic parameter depends on both the global adsorption rate and the uptake.

528 The adsorption rate of S13.5/13.5/C3(s) and NS for both pharmaceutical compounds is
529 similar. Sample S13.5/13.5/H3(s) has the highest uptake for both pollutants, in mmol
530 per gram the uptake of ibuprofen being almost twice than that of iopamidol. Compared
531 to the other two samples, carbon S13.5/13.5/H3(s) has at least twice the volume of
532 supermicropores, and a continuous micropore size distribution (Figure 5). This seems to
533 favour both the adsorption rate and the uptake of ibuprofen and iopamidol. Similar
534 results have been reported for the adsorption of paracetamol and iopamidol in sucrose-
535 derived carbons in similar experimental conditions [13].

536

537 **Table 3.** Pseudo-second order ibuprofen and iopamidol adsorption parameters at 30 ºC for
538 carbons S13.5/13.5/C3(s), S13.5/13.5/H3(s) and commercial sample (NS): k_2 is the pseudo-
539 second order rate constant; h is the initial adsorption rate; $t_{1/2}$ is the half-life time; $q_{e,calc}$ and
540 $C_{e,calc}$ are respectively, the PhC uptake and that remaining in solution at equilibrium both
541 calculated by the pseudo-second order kinetic model.

Sample	k_2 (g mg^{-1} h^{-1})	R^2	h (mg g^{-1} h^{-1})	$t_{1/2}$ (h)	$q_{e,calc}$ (mg g^{-1})	$q_{e,calc}$ (mmol g^{-1}) [a]	$C_{e,calc}$ (mg dm^{-3})
Ibuprofen							
S13.5/13.5/C3(s)	0.020	0.984	1568	0.175	280	1.365	124
S13.5/13.5/H3(s)	0.052	0.999	7127	0.052	372	1.813	106
NS	0.013	0.998	1095	0.270	296	1.443	121
Iopamidol							
S13.5/13.5/C3(s)	0.109	0.998	6513	0.037	245	0.315	131
S13.5/13.5/H3(s)	0.007	0.999	4088	0.193	787	1.013	23
NS	0.099	0.991	14704	0.026	385	0.495	77

542 [a] Calculated considering the molecular weight of ibuprofen anion and iopamidol monomers.

543 Confronting the micropore size distributions (Figure 5) with the critical dimensions of
544 the pollutants (smallest section of the most stable configuration computed in aqueous
545 solution, highlighted in bold in Figure 7), it can be concluded that ibuprofen molecule
546 (critical dimension - 0.72 nm) [47] can be easily adsorbed on the three carbons, while
547 iopamidol (critical dimensions of 0.6, 1.2 or 1.5 nm, for the monomer, dimer or trimer,
548 respectively) [48] presents diffusional constrains for most of them, with the exception of
549 sample S13.5/13.5/H3(s) due to its continuous micropore size distribution. It is
550 interesting to note that carbon S13.5/13.5/C3(s) presents the lowest iopamidol uptake;
551 this could be explained by the negligible contribution of micropores wider than 1.2 nm,
552 that would allow the adsorption of iopamidol monomers but not dimers and trimers.
553 Additionally, the mesoporosity of this carbon is not capable of accommodating the
554 bulky iopamidol aggregates (dimers, trimers or even bigger aggregates), due to the

555 average mesopore size (Fig. S6) and the above-mentioned pore-blocking effects (Fig.
556 3(b)). As a result, iopamidol removal on carbon S13.5/13.5/C3(s) does not follow the
557 expected correlation with $V_{\alpha\ super} + V_{meso}$ reported in the literature [13, 48]. It should also
558 be pointed out that in the case of carbon S13.5/13.5/C3(s) the concentration of
559 iopamidol remaining in solution at equilibrium is higher than 100 mg dm^{-3}; according to
560 molar conductivities measurements [48], this is indicative of the presence of iopamidol
561 molecular aggregates that would not accommodate in the micropores of this sample
562 (Fig. 5). Bearing this in mind, it can be inferred that the high iopamidol uptake on
563 samples S13.5/13.5/H3(s) and NS is favoured due to the presence of wider micropores
564 that allow to achieve lower equilibrium concentration in solution (*ca.* 23 and 77 mg dm^{-3}
565 , respectively) preventing the formation of molecular aggregates in solution.

566 The equilibrium adsorption isotherms presented in Figure 8 are characterized by an
567 initial rise followed by a slight continuous increase or a plateau depending on the
568 system. The experimental data were fitted to the non-linear forms of the Langmuir [32]
569 and Freundlich [33] equations; the fitting parameters, the adjusted coefficients of
570 determination and reduced chi-square values are presented in Table 4.

571 In the case of ibuprofen, the three carbons present similar F-type curves, with ibuprofen
572 uptake of sample S13.5/13.5/H3(s) being twice as big as that of carbon NS in the range
573 of assayed concentrations. This is an agreement with the total micropore volumes of the
574 adsorbents. F-type isotherms are indicative of multilayer adsorption in the sample,
575 which would allow higher adsorption capacities with increasing the ibuprofen
576 concentration in solution [33].

577 For iopamidol all the carbons show a steep initial rise in the isotherm, characteristic of a
578 high affinity between the adsorbate and adsorbent. As in the case of ibuprofen, sample

S13.5/13.5/H3(s) stands out with a remarkably high adsorption capacity whereas sample S13.5/13.5/C3(s) attains half the adsorption capacity of the commercial carbon NS. Comparing the isotherms obtained for both PhCs, it is clear that iopamidol has higher affinity for tested adsorbents than ibuprofen.

Regarding equilibrium data (Table 4) the adjusted coefficients of determination (R^2_{Adj}) and reduced chi-square values (χ^2_{Red}) indicate a good fitting to the Freundlich model for all the systems. For the particular case of iopamidol adsorption on carbons S13.5/13.5/H3(s) and S13.5/13.5/C3(s), the R^2_{Adj} and χ^2_{Red} values for Langmuir and Freundlich fittings are very close; this indicates that both models can describe the experimental data.

Table 4. Fitting parameters to the Langmuir and Freundlich models and chi-square test analysis, $\chi^2_{Reduced}$. Langmuir parameters: q_m - monolayer adsorption capacity, K_L – Langmuir constant. Freundlich parameters: K_F – Freundlich constant ($mg^{1-1/n}(dm^3)^{1/n}\ g^{-1}$), n – Freundlich exponent.

Sample	Langmuir equation				Freundlich equation			
	q_m (mg g^{-1})	K_L (dm^3 mg^{-1})	R^2_{Adj} [a]	χ^2_{Red} [b]	1/n	K_F (mg$^{1-1/n}$ (dm^3)$^{1/n}$ g^{-3})	R^2_{Adj} [a]	χ^2_{Red} [b]
Ibuprofen								
S13.5/13.5/C3(s)	278	0.032	0.358	3300	0.167	94.2	**0.669**	**1700**
S13.5/13.5/H3(s)	309	0.586	0.703	4334	0.186	140.9	**0.878**	**1785**
NS	195	0.064	0.839	546	0.333	36.9	**0.948**	**175**
Iopamidol								
S13.5/13.5/C3(s)	219	3.042	0.386	3481	0.053	173	**0.389**	**3462**
S13.5/13.5/H3(s)	965	3.109	0.881	19527	0.122	634	**0.902**	**15972**
NS	447	0.758	0.368	11023	0.040	351	**0.763**	**4139**

[a] R^2_{Adj} – Adjusted coefficient of determination accounts for the degrees of freedom (DOF)

[b] χ^2_{Red} – Reduced chi-square obtained by dividing the residual sum of squares (RSS) by the degrees of freedom (DOF)

It should be mentioned that the water solubilities of ibuprofen sodium salt (ca. 100 000 mg dm^{-3}) and iopamidol (ca. > 200 000 mg dm^{-3}) [47]) are much higher than the range

of concentrations used in this study. Thus, this parameter is not expected to affect the different adsorption trends in the adsorption of these compounds.

Adsorption capacities are also expressed in mmol of PhC per gram of carbon (Table 5), to facilitate data comparison due to the differences in the molecular weights of ibuprofen and iopamidol. Using these units, it can be observed that carbon S13.5/13.5/H3(s) presents similar uptake of ibuprofen and iopamidol, despite the lower dimension of the former. This has to be attributed to the anionic character of ibuprofen at neutral pH, which would favor the interactions with water while decreasing affinity for adsorption.

Table 5. Amount of pharmaceutical compounds adsorbed for an equilibrium concentration in solution (C_e) of 90 mg dm^{-3}. Values calculated from the fitting of the equilibrium adsorption data to Freundlich equation.

Sample	$q_{90\ mg\ dm\text{-}3}$ Ibuprofen		$q_{90\ mg\ dm\text{-}3}$ Iopamidol	
	(mg g^{-1})	(mmol g^{-1}) [a]	(mg g^{-1})	(mmol g^{-1}) [a]
S13.5/13.5/C3(s)	200	0.975	220	0.283
S13.5/13.5/H3(s)	325	1.584	1097	1.412
NS	165	0.804	420	0.540

[a] Calculated considering the molecular weight of ibuprofen anion and iopamidol monomers.

Ibuprofen uptake (in mmol g^{-1}) of S13.5/13.5/C3(s) is 3-times larger than that of iopamidol, most certainly due to diffusional constrains in the monomodal micropore network of this carbon centered at around 0.6-0.7 nm, which only allows the adsorption of iopamidol monomers and ibuprofen ions. The low iopamidol adsorption capacity (in mmol g^{-1}) of S13.5/13.5/C3(s) compared to S13.5/13.5/H3(s) and carbon NS demonstrates that when dealing with the adsorption of bulky molecules, it is essential to characterize the mesopore network. In fact, the complex mesopore network of sample S13.5/13.5/C3(s) would hinder the adsorption of iopamidol species, due to the sieving effects in the ink-bottle shape mesopores.

619 The effect of surface chemistry in the adsorption process must also be considered,
620 particularly considering the different ionic state of ibuprofen and iopamidol. At the
621 conditions of herein reported adsorption studies (aqueous solutions at pH 5) the surface
622 of carbon S13.5/13.5/C3(s) is slightly negatively charged and ibuprofen is an anion,
623 thus the results seem to point out that π-π interactions predominate over electrostatic
624 ones. Similarly, iopamidol is a neutral molecule thus the role of electrostatic
625 interactions can be disregarded. In the case of the commercial carbon, the surface is
626 slightly positively charged (pH_{PZC} of 8.4) and it presents a larger fraction of micropores
627 compared to carbon S13.5/13.5/C3(s). Its slightly lower ibuprofen adsorption capacity
628 thus confirms the hypothesis of a higher contribution of π-π interactions over
629 electrostatic ones in the adsorption of ibuprofen.

630 ## 4. Conclusion

631 We herein propose a two-step method for the valorization of a low density biomass
632 waste (sisal, *Agave sisalana*) through the synthesis of acid-chars with varied density and
633 morphology. The oxygen-rich surface and acidic nature of the acid-chars contributes to
634 increase their reactivity during the activation step, making them excellent precursors for
635 the preparation of high density nanoporous carbons with tailored pore structure in the
636 full micro-mesopore range. This approach rendered carbon materials with better porous
637 development when compared to the chemical activation of the same biomass precursor
638 by traditional methods [42, 43]. Furthermore, these adsorbents outperformed
639 nanoporous carbons commercialized for water remediation purposes, in terms of
640 adsorption capacity and rate of two pharmaceutical compounds (ibuprofen and
641 iopamidol). Both the acid-chars and their corresponding activated carbons display
642 interesting textural, morphological and surface properties that make them promising
643 materials for other applications in the fields of energy storage, catalysis, and as

644 electrode materials or supports of (bulky) molecules. In this regard, so far acid-chars
645 have proven to be effective supports for the immobilization molybdenum catalysts for
646 solventless olefins epoxidation [51].

647 **Acknowledgements**

648 This work was developed under the financial support of projects
649 UID/MULTI/00612/2013 (CQB) and UID/ QUI/50006/2013 -
650 POCI/01/0145/FERDER/007265 (REQUIMTE) from FCT/MEC through national funds
651 and co-financed by FEDER, under the Partnership Agreement PT2020. ASM thanks
652 FCT for a Post-doctoral grant SFRH/BPD/86693/2012. The authors thank Cordex for
653 supply of the sisal residues, Salmon & Cia for the supply of carbon NS, and Hovione
654 for the supply of iopamidol.

655

656 **References**

657 [1] Roskill Report, The Economics of Activated Carbon. Roskill Information Services,
658 Ltd., Claphham Road, London, 1998.

659 [2] H. Marsh, F. Rodríguez-Reinoso, Activated Carbon, Elsevier, Oxford, 2006.

660 [3] K. Schaeffer, Activated carbon 2013 market update or, the carbon convolution, in:
661 Water Conditioning & Purification, 2013.

662 [4] O. Ioannidou, A. Zabaniotou, Agricultural residues as precursors for activated
663 carbon production - A review, Renew. Sust. Energ. Rev., 11 (2007) 1966-2005.

664 [5] M.A. Yahya, Z. Al-Qodah, C.W.Z. Ngah, Agricultural bio-waste materials as
665 potential sustainable precursors used for activated carbon production: A review, Renew.
666 Sust. Energ. Rev., 46 (2015) 218-235.

667 [6] A. Jain, R. Balasubramanian, M.P. Srinivasan, Hydrothermal conversion of biomass
668 waste to activated carbon with high porosity: A review, Chem. Eng. J., 283 (2016) 789-
669 805.

[7] V.K. Gupta, A. Nayak, B. Bhushan, S. Agarwal, A Critical Analysis on the Efficiency of Activated Carbons from Low-Cost Precursors for Heavy Metals Remediation, Crit. Rev. Environ. Sci. Technol., 45 (2015) 613-668.

[8] A.M. Abioye, F.N. Ani, Recent development in the production of activated carbon electrodes from agricultural waste biomass for supercapacitors: A review, Renew. Sust. Energ. Rev., 52 (2015) 1282-1293.

[9] A.S. Mestre, A.P. Carvalho, Nanoporous carbons synthesis: an old story with exciting new chapters, in: T. Ghrib (Ed.) Porosity, IntechOpen, April 26th 2018. DOI: dx.doi.org/10.5772/intechopen.72476

[10] C. Falco, J.P. Marco-Lozar, D. Salinas-Torres, E. Morallón, D. Cazorla-Amorós, M.M. Titirici, D. Lozano-Castelló, Tailoring the porosity of chemically activated hydrothermal carbons: Influence of the precursor and hydrothermal carbonization temperature, Carbon, 62 (2013) 346-355.

[11] M. Sevilla, A.B. Fuertes, R. Mokaya, High density hydrogen storage in superactivated carbons from hydrothermally carbonized renewable organic materials, Energ. Environ. Sci., 4 (2011) 1400-1410.

[12] A.J. Romero-Anaya, M. Ouzzine, M.A. Lillo-Ródenas, A. Linares-Solano, Spherical carbons: Synthesis, characterization and activation processes, Carbon, 68 (2014) 296-307.

[13] A.S. Mestre, E. Tyszko, M.A. Andrade, M. Galhetas, C. Freire, A.P. Carvalho, Sustainable activated carbons prepared from a sucrose-derived hydrochar: remarkable adsorbents for pharmaceutical compounds, RSC Adv., 5 (2015) 19696-19707.

[14] A.S. Mestre, C. Freire, J. Pires, A.P. Carvalho, M.L. Pinto, High performance microspherical activated carbons for methane storage and landfill gas or biogas upgrade, J. Mater. Chem. A, 2 (2014) 15337-15344.

[15] M. Nunes, I.M. Rocha, D.M. Fernandes, A.S. Mestre, C.N. Moura, A.P. Carvalho, M.F.R. Pereira, C. Freire, Sucrose-derived activated carbons: electron transfer properties and application as oxygen reduction electrocatalysts, RSC Adv., 5 (2015) 102919-102931.

[16] M.-M. Titirici, R.J. White, C. Falco, M. Sevilla, Black perspectives for a green future: hydrothermal carbons for environment protection and energy storage, Energ. Environ. Sci., 5 (2012) 6796-6822.

[17] L. Wang, Y. Guo, Y. Zhu, Y. Li, Y. Qu, C. Rong, X. Ma, Z. Wang, A new route for preparation of hydrochars from rice husk, Bioresource Technol., 101 (2010) 9807-9810.

[18] M. Andrade, J.B. Parra, M. Haro, A.S. Mestre, A.P. Carvalho, C.O. Ania, Characterization of the different fractions obtained from the pyrolysis of rope industry waste, J. Anal. Appl. Pyrol., 95 (2012) 31-37.

[19] L. Wang, Y. Guo, B. Zou, C. Rong, X. Ma, Y. Qu, Y. Li, Z. Wang, High surface area porous carbons prepared from hydrochars by phosphoric acid activation, Bioresource Technol., 102 (2011) 1947-1950.

[20] M. Jorda-Beneyto, D. Lozano-Castello, F. Suarez-Garcia, D. Cazorla-Amoros, A. Linares-Solano, Advanced activated carbon monoliths and activated carbons for hydrogen storage, Micropor. Mesopor. Mater., 112 (2008) 235-242.

[21] AWWA Standard for Powdered Activated Carbon, in, American Water Works Association, Denver, Colorado, 1996.

[22] CEFIC, Test methods for activated carbon, in, Conseil Européen des Fédérations de l'Industrie Chimique (European Council of Chemical Manufacturers' Federation), 1986.

[23] J.S. Noh, J.A. Schwarz, Estimation of the point of zero charge of simple oxides by mass titration, J. Colloid Interf. Sci., 130 (1989) 157-164.

[24] M. Thommes, K. Kaneko, A.V. Neimark, J.P. Olivier, F. Rodriguez-Reinoso, J. Rouquerol, K.S.W. Sing, Physisorption of gases, with special reference to the evaluation of surface area and pore size distribution (IUPAC Technical Report), Pure Appl. Chem., 87 (2015) 1051-1069.

[25] J. Rouquerol, P. Llewellyn, F. Rouquerol, Is the bet equation applicable to microporous adsorbents?, in: P.L. Llewellyn, F. Rodriquez-Reinoso, J. Rouqerol, N. Seaton (Eds.) Studies in Surface Science and Catalysis, Elsevier, 2007, pp. 49-56.

[26] ISO9277, Determination of Specific Surface Area of Solids by Gas Adsorption - BET Method, Second Ed., in, ISO, Switzerland, 2010.

[27] F. Rouquerol, J. Rouquerol, K. Sing, Adsorption by Powders and Porous Solids - Principles, Methodology and Applications, Academic Press, San Diego, 1999.

[28] F. Rodriguez-Reinoso, J.M. Martin-Martinez, C. Prado-Burguete, B. McEnaney, A standard adsorption isotherm for the characterization of activated carbons, J. Phys. Chem., 91 (1987) 515-516.

[29] J. Jagiello, J.P. Olivier, 2D-NLDFT adsorption models for carbon slit-shaped pores with surface energetical heterogeneity and geometrical corrugation, Carbon, 55 (2013) 70-80.

[30] M.L. Pinto, A.S. Mestre, A.P. Carvalho, J. Pires, Comparison of Methods to Obtain Micropore Size Distributions of Carbonaceous Materials from CO_2 Adsorption Based on the Dubinin-Radushkevich Isotherm, Ind. Eng. Chem. Res., 49 (2010) 4726-4730.

[31] Y.-S. Ho, Review of second-order models for adsorption systems, J. Hazard. Mater., 136 (2006) 681-689.

[32] I. Langmuir, The adsorption of gases on plane surfaces of glass, mica and platinum, J. Am. Chem. Soc., 40 (1918) 1361-1403.

[33] H.M.F. Freundlich, Over the adsorption in solution, J. Phys. Chem., 57 (1906) 385-470.

[34] T.J. Bandosz, C.O. Ania, Surface chemistry of activated carbons and its characterization, in: T.J. Bandosz (Ed.) Activated Carbon Surfaces in Environmental Remediation, Elsevier, New York, 2006, pp. 159-229.

[35] B. Ruiz, I. Cabrita, A.S. Mestre, J.B. Parra, J. Pires, A.P. Carvalho, C.O. Ania, Surface heterogeneity effects of activated carbons on the kinetics of paracetamol removal from aqueous solution, Appl. Surf. Sci., 256 (2010) 5171-5175.

[36] S. Biniak, G. Szymanski, J. Siedlewski, A. Swiatkowski, The characterization of activated carbons with oxygen and nitrogen surface groups, Carbon, 35 (1997) 1799-1810.

[37] P.E. Fanning, M.A. Vannice, A DRIFTS study of the formation of surface groups on carbon by oxidation, Carbon, 31 (1993) 721-730.

[38] H. Yu, S. Niu, C. Lu, J. Li, Y. Yang, Sulfonated coal-based solid acid catalyst synthesis and esterification intensification under ultrasound irradiation, Fuel, 208 (2017) 101-110.

[39] M.-M. Titirici, M. Antonietti, Chemistry and materials options of sustainable carbon materials made by hydrothermal carbonization, Chem. Soc. Rev., 39 (2010) 103-116.

[40] International Center for Diffraction Data. Power Diffraction File Alphabetical Index; International Center for Diffraction Data, in, Swarthmore PA, 1988.

[41] M. Thommes, K.A. Cychosz, Physical adsorption characterization of nanoporous materials: progress and challenges, Adsorption, 20 (2014) 233-250.

[42] A.S. Mestre, A.S. Bexiga, M. Proença, M. Andrade, M.L. Pinto, I. Matos, I.M. Fonseca, A.P. Carvalho, Activated carbons from sisal waste by chemical activation with K_2CO_3: Kinetics of paracetamol and ibuprofen removal from aqueous solution, Bioresource Technol., 102 (2011) 8253-8260.

[43] M.A. Andrade, R.J. Carmona, A.S. Mestre, J. Matos, A.P. Carvalho, C.O. Ania, Visible light driven photooxidation of phenol on TiO_2/Cu-loaded carbon catalysts, Carbon, 76 (2014) 183-192.

[44] M.A. Andrade, A.S. Mestre, C.O. Ania, A.P. Carvalho (unpublished work) 2018.

[45] S.C.R. Marques, A.S. Mestre, M. Machuqueiro, A.Ž. Gotvajn, M. Marinšek, A.P. Carvalho, Apple tree branches derived activated carbons for the removal of β-blocker atenolol, Chem. Eng. J., 345 (2018) 669-678.

[46] J. Wang, S. Kaskel, KOH activation of carbon-based materials for energy storage, J. Mater. Chem., 22 (2012) 23710-23725.

[47] A.S. Mestre, R.A. Pires, I. Aroso, E.M. Fernandes, M.L. Pinto, R.L. Reis, M.A. Andrade, J. Pires, S.P. Silva, A.P. Carvalho, Activated carbons prepared from industrial pre-treated cork: Sustainable adsorbents for pharmaceutical compounds removal, Chem. Eng. J., 253 (2014) 408-417.

785 [48] A.S. Mestre, M. Machuqueiro, M. Silva, R. Freire, I.M. Fonseca, M.S.C.S. Santos,
786 M.J. Calhorda, A.P. Carvalho, Influence of activated carbons porous structure on
787 iopamidol adsorption, Carbon, 77 (2014) 607-615.

788 [49] M. Galhetas, A.S. Mestre, M.L. Pinto, I. Gulyurtlu, H. Lopes, A.P. Carvalho, Chars
789 from gasification of coal and pine activated with K_2CO_3: Acetaminophen and caffeine
790 adsorption from aqueous solutions, J. Colloid Interf. Sci., 433 (2014) 94-103.

791 [50] A.S. Mestre, J. Pires, J.M.F. Nogueira, A.P. Carvalho, Activated carbons for the
792 adsorption of ibuprofen, Carbon, 45 (2007) 1979-1988.

793 [51] C. Petit, M.V. Silva, A.S. Mestre, C.O. Ania, P.D. Vaz, A.P. Carvalho, C.D.
794 Nunes, Sisal derived acid-char as support of Mo(II) complex for solventless olefin
795 epoxidation, ChemistrySelect, (2018) DOI: 10.1002/slct.201802055.

796